# Label-free in-flow detection of receptor recognition motifs on the biomolecular corona of nanoparticles†

M. Gianneli, [ID] [a] E. Polo, [b] H. Lopez, [ID] [b] V. Castagnola, [b] T. Aastrup*[a] and K. A. Dawson*[b]

Nanomedicine, nanotargeting and nanotherapeutics have in the last few years faced several difficulties in translating the promising results obtained *in vitro* to an *in vivo* scenario. The origin of this discrepancy might be found in the lack of a detailed and realistic characterization of the biological surface of nanoparticles. Despite the capability to engineer nanomaterials with a great variety and a precise control of the surface functionalization, the targeting capability is lost when the nanoparticles are embedded in complex biological media, due to the formation of a biological layer (biomolecular corona). This biological layer represents the ultimate nanoparticle surface, likely to interact with the cell machinery. Therefore, in addition to traditional nanoparticle characterization techniques, a more insightful investigation of the biomolecular corona is needed, including the capability to assess the orientation and functionality of specific key molecular features. Here we present a method for the rapid screening of exposed protein recognition motifs on the surface of nanoparticles exploiting quartz crystal microbalance (QCM). We quantify accessible functional epitopes of transferrin-coated nanoparticles and correlate them to differences in nanoparticle size and functionalization. The target recognition occurs label free *in flow*, thereby pushing our investigation into a more *in vivo*-like scenario. Our method is applicable to a wide array of nanoparticles and therefore holds the potential to become an advanced technique for the classification of all kinds of nanobioconstructs based on their biological external functionality.

## Introduction

In recent years, nanoparticles (NPs) have found widespread use in the biomedical field[1] as carriers, as labelling and tracking agents, as vectors for gene therapy,[2,3] in hyperthermia treatments and as magnetic resonance imaging (MRI) contrast agents,[4,5] and they still hold great potential to improve medical therapeutics and diagnostics.[6–8] However, in order to apply them in these contexts, the fundamental interactions that drive biological processes once nanomaterials come into contact with living systems should be carefully investigated.[9,10] It is now well accepted that, upon incorporation *via* the lungs, gut or skin, NPs interact with extracellular biomolecules dissolved in biological fluids, including proteins, sugars and lipids, producing a bio-nanointerface known as "biomolecular corona".[11–13] This biological layer provides the NPs with a new external surface capable of interacting with the cells and biological barriers at the receptor level.[14–16] In this respect, it has been shown that a key role is played by the organization and orientation of the proteins that compose this biomolecular corona.[14,17–20] The protein composition and conformational structure of this layer critically depend on and can be modulated by the NP properties, such as size, shape and surface chemistry.[21,22] In addition, the need to deliver NPs to specific organs and tissues by targeting selective cellular receptors has made researchers achieve great advances in engineering a plethora of targeting NP designs for therapeutic purposes. The high control over the synthesis and functionalization of NPs decorated with a variety of bio-(molecules) arranged in specific ways on their surface may induce receptor-mediated cell internalization and modulate intracellular trafficking. However, despite their huge potential and the recent advances, limited success in targeting has been achieved and the clinical translation of nanotherapeutics still remains a challenge.[23,24] A discrepancy between *in vitro* and *in vivo* experiments is often found. The lack of detailed understanding of the NP biological surface (including composition, organization and activity/func-

[a]*Attana AB, Greta Arwidssons Väg 21, SE-11419 Stockholm, Sweden*
[b]*Centre for BioNano Interactions, School of Chemistry and Chemical Biology, University College Dublin, Belfield, Dublin 4, Dublin, Ireland.*
*E-mail: kenneth.a.dawson@cbni.ucd.ie*
†Electronic supplementary information (ESI) available. See DOI: 10.1039/c7nr07887k

tionality of the exposed biomolecules) is probably at the origin of this failure. Besides, the demonstrated functionality of NPs *in vitro* (in simplified model environments) is insufficient to predict their *in vivo* targeting capabilities, where the challenges associated with the complexity of the scenario increase highly. NPs can be rapidly covered by another dynamic layer of biomolecules from the environment and this final layer might lead the NP clearance process by liver, kidneys, *etc.*[25] In addition, body fluids are dynamic in nature so the question arises whether the experimental conditions, *e.g.* dynamic flow *vs.* static incubation, affect the NP–biomolecule fingerprints.[26]

The physico-chemical characterization of NPs is insufficient to describe and/or predict NP–protein, NP–protein–protein, and NP–cell interactions. Several characterization techniques (dynamic light scattering, differential centrifugal sedimentation, fluorescence correlation spectroscopy, *etc.*)[27–30] in combination with proteomics and biophysical methods have increased our understanding on NP–protein interactions. Functional motifs presented at the periphery of the NP surface are of paramount importance for a detailed understanding of the processes involved at the molecular level,[31] in order to assess the quality of the targeting capabilities of NPs before moving to *in vivo* experiments. Therefore, the development of new tools and approaches to fully characterize the bio-nano-interface in detail,[32–34] including the microscopic mapping of molecular motifs presented on the NP surface, is now urgently needed and some approaches based on immunolabelling have been recently reported.[19,20] However, in all these approaches, recognition takes place under static (bulk) conditions.

Quartz microbalance (QCM) can exploit immunometric techniques for the precise detection of biomolecules and the use of NPs often allows the amplification of the signal.[35–37] Here we apply QCM for the detection of specific NP recognition epitopes, introducing a fast, label-free screening methodology for mapping the NP biological surface. QCM allows for the rapid assessment of biological interactions without the need for any further probes that may modify the surface functionality of NPs, therefore eliminating any perturbation to the system. It is also not limited by the nanomaterial chemical composition, and hence holds the potential to become a routine characterization technique for bio-nanoconstructs. Moreover, since the recognition occurs *in flow*, it reflects more realistic *in vivo*-like conditions where the NPs flowing in the blood vessels are seen and recognised by cellular receptors.

In this work, polystyrene (PS) NPs (and gold NPs) of different sizes and surface functionalizations were incubated with human *holo*-Transferrin (Tf) leading to a physically adsorbed protein corona. Using appropriate monoclonal antibodies and a QCM "sandwich" biochemical assay format, we could quantify surface-exposed protein recognition epitopes and link them to the different physical chemical properties of the NPs. The estimated number of these epitopes was compared to previously reported data where epitope quantification was realized under static experimental conditions (*e.g.* incubation) and the influence of the flow rate on target recognition was investigated. Moreover, the washing steps performed in flow significantly shortened the analysis time, inducing a minimal system perturbation when compared to traditional centrifugation-based washing techniques.

## Results and discussion

### Experimental setup

Colloidal dispersions of different types of NPs were incubated for 1 h at 37 °C with human transferrin (Tf) as the model protein (see the ESI, Scheme 1†) to form a biomolecular corona.[38] The so-produced NP-Tf complexes were washed by centrifugation steps to remove unabsorbed proteins and were resuspended in phosphate buffer saline (PBS). The resulting suspensions were then fully characterized using differential centrifugal sedimentation (DCS), dynamic light scattering (DLS) and nanotracking analysis (NTA) (see the ESI, Fig. S1–S2 and Tables S1–S2†).

In parallel, QCM LNB-carboxyl sensor chips (Attana AB, Sweden) were functionalized through conventional amine coupling chemistry (*via* EDC-NHS) with a monoclonal antibody anti-Tf (mAb-Tf, see Fig. S4†) that recognizes an epitope proximate to the Tf receptor-binding region (Pro142-Pro145).[19]

The successful immobilization of the mAb-Tf was assessed by a similar Ab surface sensor coverage, monitored by the change of frequency after the Ab immobilization step, for all experiments (see Fig. S5†). Thereafter the NP-Tf complexes in PBS were injected over the sensor surface at a selected flow rate of 10 μl min⁻¹ and the frequency changes due to the nanoparticle complex binding were monitored in real time. Depending on the type of the nanoparticle employed, *i.e.* size or surface chemistry, one or more injections of the complexes were performed so that the net frequency shift caused by the binding of the nanoparticle complexes to the immobilized antibodies was in the order of 60 to 110 Hz. For NPs of the same material and size but different functionalizations, the injection of the nanoparticle complexes was stopped once similar frequency shifts were obtained; thus similar numbers

**Table 1** Summary of the number of antibodies detected per PS NP with different sizes (100 and 200 nm) and surface chemistries (carboxylated PS NPs and sulphonated PS NPs)

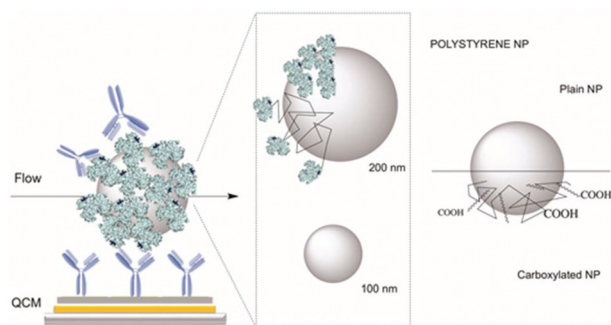| | PS SO$_3$ | | PS COOH | |
|---|---|---|---|---|
| Diameter (nm) | 100 | 200 | 100 | 200 |
| Frequency shift (Hz)$_{NPTf}$ | 153 | 66.7 | 138.5 | 62.5 |
| $M_{tot}$ (ng) | 107.1 | 46.7 | 96.9 | 43.7 |
| $M_{eff}$ (ng) $_{core\ shell\ model}$ | $4.5 \times 10^{-8}$ | $4.2 \times 10^{-7}$ | $5.0 \times 10^{-8}$ | $1.8 \times 10^{-7}$ |
| No. of NPs immobilized | $2.4 \times 10^9$ | $1.1 \times 10^8$ | $1.9 \times 10^9$ | $2.4 \times 10^8$ |
| Tf/NP (theory) | 711 | 2844 | 711 | 2844 |
| Frequency shift (Hz)$_{mAb}$ | 20 | 7.75 | 8 | 2.7 |
| $M$ Ab (ng) | 14 | 5.4 | 5.6 | 1.9 |
| Ab molecules | $5.3 \times 10^{10}$ | $2.0 \times 10^{10}$ | $2.1 \times 10^{10}$ | $7.1 \times 10^9$ |
| No. of Abs/NP | 22 | 184 | 11 | 30 |

**Fig. 1** Schematic illustration of the experimental setup for the bio-recognition assay and of the nanoparticles employed (two different sizes and two different surface chemistries for the same type of nanomaterial have been used).



**Fig. 2** Sensorgrams showing (a) the injection of PS NP-Tf complexes (I) followed by two consecutive injections of monoclonal anti-transferrin antibody mAb-Tf (IIa, IIb) and regeneration with 10 mM glycine (pH 1.5) (IIIa, IIIb) and (b) the close-up of mAb-Tf injections. In the inset, the rolling average for time windows of 20 s is presented.

of particles were immobilized (see Table 1). A second channel was used in parallel as a control/reference where no NP-Tf complexes were injected (see the ESI for the control experiments, Fig. S6–S8†). The specificity of the binding of the NP-Tf complexes to the sensor surface was assessed by performing a control experiment where injections of PS NPs incubated with BSA protein were performed. These injections resulted in negligible frequency shifts, *i.e.* no non-specific binding (Fig. S8A and B†).

After the binding of the NP complexes to the sensor surface, a "sandwich" assay was conducted using the same mAb-Tf that was previously employed as capture Ab. A schematic representation of the assay is shown in Fig. 1. The antibody was injected in both the main and reference channel. The injection was repeated twice to ensure saturation of the surface of the NP-Tf complexes, which was verified by a frequency change (Fig. 2). In the absence of nanoparticle complexes, channel B did not show any interaction with the secondary antibody (Fig. S7†). The details of the procedure are presented in the Materials and Methods section as well as in the ESI.†

Fig. 2a illustrates the different steps of the "sandwich" assay format, starting from the injection of the NP-Tf complexes while Fig. 2b is a close-up of the two consecutive secondary antibody injections. The net frequency shift due to the binding of the secondary antibody was measured 50–100 s after the completion of the second injection, when the frequency signal had been stabilized. Notice that the fluctuation of the signal is less than 0.2 Hz and that the rolling average (the average of the frequency using time windows of 20 s) for a 125 s period did not show a drift of the signal (see the insert of Fig. 2b). Both observations confirm that the signal was indeed stabilized and reached a constant value. This frequency shift allowed for the determination of the number of immobilized antibody molecules per NP-Tf complex (see Table 1). The successful immobilization of NP complexes on the sensor chip surface was also verified by SEM at the end of the experiment and before the regeneration step (Fig. S14†). The total duration of the assay was 30 min, which allows for the analysis and comparison of several different NP types in a limited time frame.
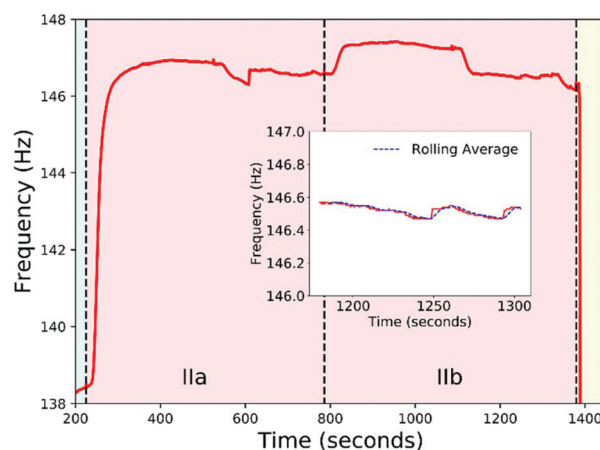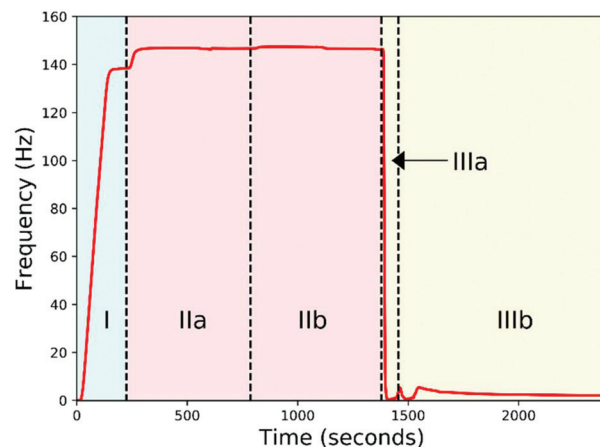
### Calculation of the total number of Tf receptor-binding motifs

The total mass of immobilized NP-Tf complexes was calculated by the net frequency shift obtained after the injection of the complexes. Each Tf-coated NP is composed of a core of diameter ($D_c$) and density ($\rho_c$), and a Tf layer of thickness ($s$) and density ($\rho_s$). The full particle complex has a total diameter $D_T = D_c + 2s$. Therefore a core–shell model based on DCS measurements previously developed was used to analyse the data for protein (shell) coated particles in order to estimate the shell thickness.[39] By applying this model to the data obtained from the characterization of 200 nm PS NP (with and without Tf) by DCS, we could determine the Tf thickness layer (~3 nm, which is assumed to be constant for all calculations) and we could calculate the effective mass $M_{eff}$ of such NP-Tf complexes (see Table 1 and the ESI, eqn (3)†). This allowed the estimation of the total number of particles immobilized on the sensor surface, $N = M_{tot}/M_{eff}$ where $M_{tot}$ is given by the change of frequency times 0.7 ng (mass corresponding to 1 Hz of frequency shift). In a similar way, the frequency shift obtained after the injection of the secondary antibody allowed for the determi-

nation of the number of immobilized antibody molecules per NP-Tf complex (see Fig. S11–S12 and Table S3†). In Table 1 the results obtained for the mapping of PS NP-Tf complexes of a nominal core diameter of 100 nm and 200 nm with both plain (–SO$_3$ terminated) and PEGylated (–COOH terminated) surfaces are reported. As expected, the number of functional Tf epitopes recognized increased with the NP size. Notice that neither of the systems showed a quadratic growth of the number of epitopes with the diameter of the NP indicating that the trend observed is not solely due to the increase of the surface of the NP. This result indicates that besides the surface area, other physico-chemical parameters of the NP surface (roughness, surface charge and surface chemistry) might greatly influence the protein adsorption, thereby determining the multivalency of the active motifs on the NP surface.

In order to calculate the percentage of Tf oriented in a favourable way for the receptor recognition, first, the total protein coverage amount was both estimated theoretically and determined experimentally. For the theoretical calculation, a complete coverage of the NP surface with Tf was considered. Assuming that a single Tf can be considered as a sphere with radius $r = 3.75$ nm, the number of Tf on the surface of a NP of diameter $D$ is given by $D^2/r^2$. The experimental determination of the total number of adsorbed proteins per particle was carried out using intensitometry values for the SDS-PAGE bands (see Fig. S9†). The effect of the NP surface functionalization on the protein adsorption is shown in Fig. 3, where the percentage of well-oriented Tf on the NP surface that was found to bind to antibodies is shown. Two calculations are reported, assuming a dense packed layer of Tf (labelled as Tf complete coverage) and using the average of the Tf measured
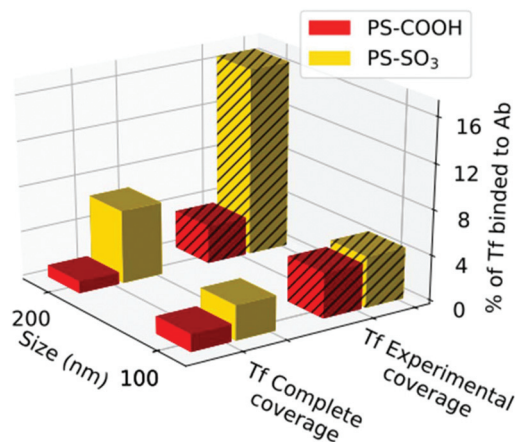


Fig. 3 Percentage of available Tf epitopes recognised by mAb-Tf for PS NPs of different sizes and surface chemistries. The percentage is calculated over the total amount of protein coverage both theoretically and experimentally determined. QCM analysis of the NP protein complexes determines the influence of the variation of the surface chemistry (–SO$_3$ and –COOH) and the NP size (100 and 200 nm) in the number of exposed Tf epitopes: size is the driving factor in the case of the 100 nm PS NP (4% of Tf for PS-SO$_3$ NP and 3% of Tf for PS-COOH NP); however surface chemistry (16% of Tf for PS-SO$_3$ NP and 3% of Tf for PS-COOH NP) seems to play a major role for 200 nm of PS NP.

by SDS-PAGE (labelled as Tf experimental coverage). The calculated percentages are less than 20% suggesting that the Tf molecules attach to the surface of the NP in a non-selective way. The difference observed between the two functionalizations confirmed that the preferred or more favourable binding orientation depends on the surface chemistry of the NP, in agreement with previous theoretical[40,41] and experimental[19,20,31] reports.

Sulphonated PS NPs exhibit a relatively hydrophobic surface, which can influence the Tf orientation when adsorbed on the NP surface. Despite the relatively similar amount of absorbed Tf for both PS NPs (approximately 1.2 times higher for the sulphonated particles than the carboxylated ones of the same size, experimentally determined by gel electrophoresis, Fig. S9†), the total number of Tf epitopes recognised by mAb-Tf is two times higher for 100 nm sulphonated PS NPs and between 4–6 times higher for 200 nm sulphonated PS NPs, when compared to carboxylated PS NPs of the same size. This highlights the necessity to not only determine the amount of protein immobilized on the NP surface but also to have a fast and robust methodology for screening the valency of active motifs exposed on the NP surface, which will define the biological activity of the NP. By modifying the size, surface curvature or surface chemistry, this number can be modulated, being capable of controlling particle–cell interactions (multivalency promotes stronger NP–cell receptor interactions, oligomerization of receptors leading to different internalization pathways, *etc.*).[42,43]

To verify that the method proposed is not limited to PS NPs, and can be directly used to study different NP materials and sizes, we also measured the Tf functional epitopes on different sizes of gold citrate capped NPs (see the ESI, Fig. S13 and Table S4† for QCM results and Table S2, Fig. S2, S3, S10† and the Experimental section for details on the synthesis and characterization).

One should note that a difference between the absolute numbers of counted epitopes obtained with the QCM-based methodology and the ones obtained with other static approaches such as immunolabelling techniques[19,20] is to be expected. First of all, QCM resembles a 2D rather than a 3D assay; part of the surface of the nanoparticle complexes is not available for binding to the secondary antibody since it is already occupied by the ligand found on the sensor chip surface. Secondly, when a large number of nanoparticle complexes are immobilized on the sensor surface, there is the risk of steric hindrance, meaning less secondary antibody could interact with the complexes. However, it is the relative number of counted functional epitopes under the same experimental conditions that is of interest here.

Making predictions about the NP biological response based solely on the NP physico-chemical attributes may result in conclusions partially true for a specific NP type or experimental design, which are not universally valid. The answer to thorough NP investigation lies in careful testing of nanomaterials under various conditions, including assessing the orientation and functionality of specific key molecular features

on their surface. For example, characterizing in detail the number of potentially active epitopes will allow one to define the NP targeting capabilities under different scenarios.[44]

The proposed method has the potential to become a routine NP characterization technique along with more classical physico-chemical characterization techniques. This methodology allows the comparison of the relative number of epitopes exposed on different NP surfaces that can be recognized by other proteins, cellular receptors, *etc*. In addition, these interactions can be evaluated in more relevant scenarios such as complex media and/or different flow rates.

### Effect of the flow rate

As mentioned previously, every intravenously administered NP is in contact not only with biological fluids and their components but also with the constituent flow-dynamic environment. The current *in vitro* techniques for the characterization of the bio-nanointerface are usually static by nature and as such ignore the shear stress produced by the blood flow and limited contact time. Early studies demonstrated that the introduction of lateral flow to a NP system can alter the balance between diffusion and sedimentation forces, thereby modifying dosimetry, NP internalization, and bio-responses.[45,46]

An additional advantage of the method presented here is the ability to control the flow conditions by varying the flow rate. For the experimental setup used and the accessible flow rates of the instrument (between 2 and 150 µl min$^{-1}$) we estimate the Reynolds numbers for the flow inside the channel in the range 0.01–1 which is in the same order of the Reynolds numbers determined for the flow of blood in arterioles, capillaries and venules.[47] In this sense, the possibility to detect receptor binding motifs available at the NP surface for potential engagement with specific cell receptors in a small volume under continuous flow places our methodology a step forward towards more realistic blood vessel conditions.[48,49]

To study the influence of flow rate on antibody recognition and therefore on the number of Tf epitopes detected, we now report experiments in which the flow conditions are varied during the mAb-Tf injection step. Four different flow rates were used: 5, 7, 10 and 25 µl min$^{-1}$. As shown in Fig. 4, no influence of the flow rate on the recognition was detected as the mean number of mAb-Tf per NP (2 replicates in each case) is constant for the flow rate range employed. This result indicates that, for our microchannel structure and the operation conditions used, the transport of antibodies is diffusion dominated.

Moreover, the method reported here is flexible and suitable for further optimization including the possibility to control flow conditions to more accurately mimic *in vivo* NP exposure. For instance, increasing the flow rate to a value where convective transport dominates could be used to study epitope accessibility in out-of-equilibrium situations and, in addition, could further shorten the experimental measurement time.
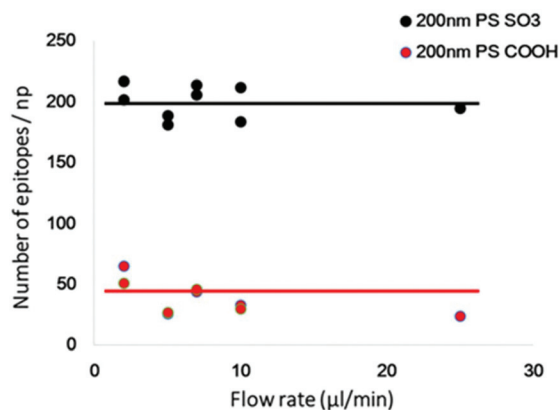


**Fig. 4** Influence of the flow rate on the number of epitopes detected per 200 nm PS NPs.

## Conclusions

A quantitative understanding of the NP–cell interaction is an important prerequisite for successfully designing and engineering NPs with enhanced or suppressed cellular effects. It is well accepted that when nanomaterials are in contact with biofluids, the biomolecules that naturally adsorb onto their surface represent the final functional surface likely to engage with the cells. Despite being able to link the biomolecular composition to the core material and the chemical surface, the orientation of specific proteins or motifs on the NP surface is poorly characterized.

Here we present a robust quantitative methodology to measure receptor recognition motifs of NP–biomolecule complexes under relevant conditions. This characterization assay enables the determination of the specific orientation of the proteins and therefore will predict the functionality and availability of specific epitopes of interest.

This biological characterization must be included in the routine nanoparticle batch characterization, in addition to more classical physical-chemical characterization. In order to develop a high-throughput analysis for the quality control of all kinds of natural and engineered nanobioconstructs, it is essential to apply cost- and time-effective protocols. The methodology outlined here represents a fast and reliable way of screening the biological surface of NPs in flow, using low volumes and a label-free readout.

The washing steps performed in the flow greatly shorten the time of analysis, inducing a minimal perturbation of the system if compared to traditional washing techniques based on centrifugation. Thus, the screening of a variety of nanomaterials can be realized in a short time.

Moreover, since the recognition occurs in a continuous flow, it makes the system similar to the blood vessel environment. The NPs in biomedical applications are administered mostly systemically and enter the blood stream subjected to different flow rates and flow regimes. In this work, we could mimic flow rates commonly found in arterioles, capillaries,

and venules but the technique holds great potential for future developments and optimization in this regard.

Finally, the possibility to perform the analysis *in situ* (including highly complex dispersions and relevant biological milieu) will represent an important step for the acquisition of detailed molecular information in realistic biological scenarios, potentially allowing to detect and consider also "softer" interactions.

In conclusion, the method presented here is an important tool for advanced NP characterization, allowing to obtain the biological fingerprint of NPs that will likely define their biological outcomes (targeting specific cellular receptors, internalization pathways, *etc.*). The systematic use of this characterization tool will pave the way for a more conscious NP design that will represent a great improvement in the field of nanomedicine, targeting and diagnosis.

## Methods

### Materials

All chemicals were of the highest grade available and used as received. Gold(III) chloride trihydrate (520918), *O*-(2-carboxyethyl)-*O*′-(2-mercaptoethyl) heptaethylene glycol (SH-PEG-COOH, 672688), PBS tablets (P4411), Trizma® base (T1503), glycine (G8898), ammonium persulfate (A3678), ethylenediaminetetraacetic acid disodium salt dehydrate (EDTA) (252352), sodium dodecyl sulfate (SDS) (L3771), *N*,*N*,*N*′,*N*′-tetramethylethylenediamine (TEMED) (T9281), sucrose (m117), dodecane (D22110), acrylamide/bis-acrylamide 40% solution (A7802), dithiothreitol (DTT) (D5545), ethanol (32294-2), methanol (24229-2), and trisodium citrate dihydrate (S1804) were purchased from Sigma-Aldrich. In addition, PVC calibration standard 483 nm (PVC000476) was purchased from Analytik Ltd; ColorPlus Prestained Protein Ladder, Broad Range (10–230 kDa) (P7711S) and blue loading buffer for SDS-PAGE were obtained from New England Bio-Labs (cat. no. B7703S); and 2D Silver Stain Kit II [Daiichi] (167997) was purchased from Insight Biotechnology.

Proteins: Holo-Transferrin Human, Tf (T44132), was purchased from Sigma-Aldrich. Antibodies: the antibody anti-Tf (monoclonal HTF-14: ab769) was purchased from Abcam (UK) and the antibody anti-Myoglobin 7005 (IgG1) was purchased from Medix Biochemica (Finland).

Particles: Polystyrene NPs were purchased from PolySciences (2.6%Sol., 26 mg mL$^{-1}$ stock solution, 07304 200 nm plain PSNP, 00876 100 nm plain PSNP, 08216 200 nm carboxylated PSNP, 16688 100 nm carboxylated PSNP).

### Nanoparticle characterization

UV-visible spectroscopy was performed on a Cary 600i UV-visible spectrophotometer using 1 cm path length Hellmaz quartz cells, measuring in the 200–800 nm range.

Differential centrifugal sedimentation (DCS) analysis of NPs was performed using a CPS Disk Centrifuge DC2400. The measurements were carried out using a 2–8% sucrose density gradient in Milli-Q® water and PBS buffer, with the disc speed set to 24 000 rpm while monitoring in the 1–500 nm range. Each particle size measurement was calibrated using a PS standard of nominal diameter 520 nm. 100 μL of the standard was injected before each measurement to calibrate the instrument. 100 μL of the particles was injected and analysed by DCS.

For dynamic light scattering (DLS), a Zetasizer Nano ZS instrument (Malvern Instrument Ltd) was employed to study the size distribution of the NPs. Briefly, 25 μL of the NP stock was diluted to 1 mL with PBS buffer and measured.

The concentration of the NPs was measured by nanotracking analysis using a NanoSight LM10 instrument (Malvern Instrument Ltd). Briefly, 10 μL of the NP stock was diluted to 1 mL with PBS buffer and measured. The samples were measured for 60 s with manual shutter and gain adjustments. Three measurements of each sample were performed for all NPs. The mean size and SD values obtained using the NTA software correspond to the arithmetic values calculated with the values from all the particles analyzed by the software.

### Polystyrene NP coated with transferrin (PS@Tf NP)

The PS@Tf NPs were prepared fresh before each experiment. 200 nm, 100 nm and 50 nm PS NPs (1 mg) were incubated with Tf (64 nmol, 5 mg) in MES buffer (pH 6) on a shaker in order to saturate the nanoparticle surface. After 1 h of incubation at RT, the PS@Tf NPs were centrifuged at 10 000 rpm for 40 min and re-suspended in fresh buffer to remove the unbound protein. The NPs were washed two times with MES (pH 6) and two times with PBS (pH 7.4). The particles were finally re-suspended in PBS at a final concentration of 1 mg mL$^{-1}$. The NP concentration was determined by NTA before and after the purification steps necessary to remove the unbound Tf protein.

### Protein determination: polyacrylamide gel electrophoresis (SDS-PAGE)

The protein was denatured by boiling the samples for 5 minutes in a loading buffer (62.5 mM Tris-HCl (pH 6.8), 2% (w/v) SDS, 10% glycerol, 0.01% (w/v) bromophenol blue, 40 mM DTT). The prepared samples, containing denatured proteins coated with an SDS surfactant (which gives them a negative net charge), were separated by size in the moiety of porous 10% polyacrylamide gel (1D SDS-PAGE), in an electric field using a Mini-PROTEAN Tetra electrophoresis system from Bio-Rad.

SDS-PAGE (sodium dodecyl sulfate polyacrylamide electrophoresis). For two running gels: 10% SDS-PAGE gel was precast fresh before each experiment as 5.4 mL of Milli-Q® water, 2.5 mL of 1.5 M Tris-HCl buffer (pH 8.9) and 0.1 mL of 10% SDS are mixed well and to them 1.8 mL of 40% acrylamide and 5 μL of TEMED are added and the solution is mixed again. As an initiator, 50 μL of 10% ammonium persulfate is added. The gel solution is poured in the frame to polymerize. Stacking gels (4%) are made up with 0.5 mL acrylamide, 1.26 mL 0.5 M Tris-HCL buffer (pH 6.8), 50 μL 10%

SDS, 3.18 mL Milli-Q® water, 25 μL APS (10%) and 5 μL TEMED and added on top of the running gels.

The electrophoresis was run under a constant voltage of 150 V for about 45 minutes. The gels were stained with 2D Silver Stain II reagents (Cosmobio Co., Ltd) and scanned under white light using a G:Box Chemi XT4 (Syngene). ImageJ software was used to analyse the images.

### QCM binding analysis

The biosensor experiments were carried out on an Attana Cell 200 QCM biosensor (Attana AB, Stockholm, Sweden), which consists of a dual channel, flow-through system, where the running buffer is continuously flowed through the flow cell over the sensor surfaces at a given flow rate and the sample is introduced over the sensor surfaces using a six-way valve. The continuous flow of the buffer over the sensor surfaces, and the simultaneous measurement of the frequency allows for the real-time measurement of the interaction between the analyte in the buffer and the bio-macromolecule on the sensor surfaces. The two channels are referred to as channel A and channel B, where A was used for monitoring the molecular interaction and B served as a reference. Attana LNB-carboxyl sensor chip surfaces were used in this study. The Attana Cell 200 instrument features a temperature control unit (4–40 °C ± 0.1 °C). All the QCM experiments in this study were performed at 22 °C.

### Functionalization of Attana LNB-carboxyl chips with anti-Tf antibody

Two Attana LNB-carboxyl sensor chips were docked in channel A and channel B of the system and were allowed to stabilize in PBS running buffer at 100 μL min⁻¹. Then the flow rate was set to 10 μL min⁻¹ and the surfaces were activated for 10 min with a reagent mixture of EDC and sulfo-NHS. The monoclonal anti-transferrin antibody to be immobilized, dissolved in 10 mM acetic acid buffer, pH 6.0 at 50 μg mL⁻¹, was thereafter injected over the activated surfaces for a contact time of 5 min. The remaining active groups on the surfaces were deactivated with 1 M ethanolamine at pH 8.5. The immobilization of the anti-transferrin antibody on the surfaces resulted in a frequency shift of 160–200 Hz.

### QCM sandwich assay

For biochemical assay, "sandwich" format assays were developed to count the functional epitopes on the surface of NP-Tf complexes. The interaction of NPs incubated with Tf, with mAb anti-Tf immobilized on the sensor surface, was carried out in PBS at 10 μL min⁻¹. Once the NPs were captured by the functionalized surface of channel A, a solution of 100 μg mL⁻¹ of mAb anti-Tf was injected twice on both channels.

## Conflicts of interest

There are no conflicts to declare.

## Acknowledgements

## References

1 B. Pelaz, C. Alexiou, R. A. Alvarez-Puebla, F. Alves, A. M. Andrews, S. Ashraf, L. P. Balogh, L. Ballerini, A. Bestetti, C. Brendel, S. Bosi, M. Carril, W. C. W. Chan, C. Chen, X. Chen, X. Chen, Z. Cheng, D. Cui, J. Du, C. Dullin, A. Escudero, N. Feliu, M. Gao, M. George, Y. Gogotsi, A. Grünweller, Z. Gu, N. J. Halas, N. Hampp, R. K. Hartmann, M. C. Hersam, P. Hunziker, J. Jian, X. Jiang, P. Jungebluth, P. Kadhiresan, K. Kataoka, A. Khademhosseini, J. Kopeček, N. A. Kotov, H. F. Krug, D. S. Lee, C.-M. Lehr, K. W. Leong, X.-J. Liang, M. Ling Lim, L. M. Liz-Marzán, X. Ma, P. Macchiarini, H. Meng, H. Möhwald, P. Mulvaney, A. E. Nel, S. Nie, P. Nordlander, T. Okano, J. Oliveira, T. H. Park, R. M. Penner, M. Prato, V. Puntes, V. M. Rotello, A. Samarakoon, R. E. Schaak, Y. Shen, S. Sjöqvist, A. G. Skirtach, M. G. Soliman, M. M. Stevens, H.-W. Sung, B. Z. Tang, R. Tietze, B. N. Udugama, J. S. VanEpps, T. Weil, P. S. Weiss, I. Willner, Y. Wu, L. Yang, Z. Yue, Q. Zhang, Q. Zhang, X.-E. Zhang, Y. Zhao, X. Zhou and W. J. Parak, *ACS Nano*, 2017, **11**, 2313–2381.
2 T.-H. Shin, J.-s. Choi, S. Yun, I.-S. Kim, H.-T. Song, Y. Kim, K. I. Park and J. Cheon, *ACS Nano*, 2014, **8**, 3393–3401.
3 H. Yin, R. L. Kanasty, A. A. Eltoukhy, A. J. Vegas, J. R. Dorkin and D. G. Anderson, *Nat. Rev. Genet.*, 2014, **15**, 541–555.
4 M. Colombo, S. Carregal-Romero, M. F. Casula, L. Gutierrez, M. P. Morales, I. B. Bohm, J. T. Heverhagen, D. Prosperi and W. J. Parak, *Chem. Soc. Rev.*, 2012, **41**, 4306–4334.
5 H. Huang, S. Delikanli, H. Zeng, D. M. Ferkey and A. Pralle, *Nat. Nanotechnol.*, 2010, **5**, 602–606.
6 M. Ferrari, *Nat. Rev. Cancer*, 2005, **5**, 161–171.
7 J. Shi, P. W. Kantoff, R. Wooster and O. C. Farokhzad, *Nat. Rev. Cancer*, 2017, **1**, 20–37.
8 G. Chen, I. Roy, C. Yang and P. N. Prasad, *Chem. Rev.*, 2016, **116**, 2826–2885.
9 J. Lazarovits, Y. Y. Chen, E. A. Sykes and W. C. W. Chan, *Chem. Commun.*, 2015, **51**, 2756–2767.

10 E. Blanco, H. Shen and M. Ferrari, *Nat. Biotechnol.*, 2015, **33**, 941–951.

11 M. P. Monopoli, C. Åberg, A. Salvati and K. A. Dawson, *Nat. Nanotechnol.*, 2012, **7**, 779–786.

12 K. Hamad-Schifferli, *Nanomedicine*, 2015, **10**, 1663–1674.

13 T. Cedervall, I. Lynch, S. Lindman, T. Berggård, E. Thulin, H. Nilsson, K. A. Dawson and S. Linse, *Proc. Natl. Acad. Sci. U. S. A.*, 2007, **104**, 2050–2055.

14 S. Lara, F. Alnasser, E. Polo, D. Garry, M. C. Lo Giudice, D. R. Hristov, L. Rocks, A. Salvati, Y. Yan and K. A. Dawson, *ACS Nano*, 2017, **11**(2), 1884–1893.

15 Z. J. Deng, M. Liang, M. Monteiro, I. Toth and R. F. Minchin, *Nat. Nanotechnol.*, 2011, **6**, 39–44.

16 S. Ritz, S. Schottler, N. Ktoman, G. Baler, A. Musyanovych, J. Kuharev, K. Landfester, H. Schild, O. Jahn, S. Tenzer and V. Mailander, *Biomacromolecules*, 2015, **16**(4), 1311–1321.

17 A. Lesniak, F. Fenaroli, M. P. Monopoli, C. Åberg, K. A. Dawson and A. Salvati, *ACS Nano*, 2012, **6**, 5845–5857.

18 M. Lundqvist, J. Stigler, G. Elia, I. Lynch, T. Cedervall and K. A. Dawson, *Proc. Natl. Acad. Sci. U. S. A.*, 2008, **105**, 14265–14270.

19 P. M. Kelly, C. Åberg, E. Polo, A. O'Connell, J. Cookman, J. Fallon, Ž. Krpetić and K. A. Dawson, *Nat. Nanotechnol.*, 2015, **10**, 472–479.

20 M. C. Lo Giudice, L. M. Herda, E. Polo and K. A. Dawson, *Nat. Commun.*, 2016, **7**, 13475.

21 Y. Jiang, S. Huo, T. Mizuhara, R. Das, Y.-W. Lee, S. Hou, D. F. Moyano, B. Duncan, X.-J. Liang and V. M. Rotello, *ACS Nano*, 2015, **9**, 9986–9993.

22 D. Pozzi, V. Colapicchioni, G. Caracciolo, S. Piovesana, A. L. Capriotti, S. Palchetti, S. De Grossi, A. Riccioli, H. Amenitsch and A. Lagana, *Nanoscale*, 2014, **6**, 2782–2792.

23 S. Wilhelm, A. J. Tavares, Q. Dai, S. Ohta, J. Audet, H. F. Dvorak and W. C. W. Chan, *Nat. Rev. Mater.*, 2016, **1**, 16014.

24 A. Salvati, A. S. Pitek, M. P. Monopoli, K. Prapainop, F. B. Bombelli, D. R. Hristov, P. M. Kelly, C. Aberg, E. Mahon and K. A. Dawson, *Nat. Nanotechnol.*, 2013, **8**, 137–143.

25 K. M. Tsoi, S. A. MacParland, X.-Z. Ma, V. N. Spetzler, J. Echeverri, B. Ouyang, S. M. Fadel, E. A. Sykes, N. Goldaracena, J. M. Kaths, J. B. Conneely, B. A. Alman, M. Selzner, M. A. Ostrowski, O. A. Adeyi, A. Zilman, I. D. McGilvray and W. C. W. Chan, *Nat. Mater.*, 2016, **15**, 1212–1221.

26 D. Pozzi, G. Caracciolo, L. Digiacomo, V. Colapicchioni, S. Palchetti, A. L. Capriotti, C. Cavaliere, R. Zenezini Chiozzi, A. Puglisi and A. Lagana, *Nanoscale*, 2015, **7**, 13958–13966.

27 L. Shang and G. U. Nienhaus, *Acc. Chem. Res.*, 2017, **50**, 387–395.

28 Z. e. Krpetić, A. M. Davidson, M. Volk, R. Lévy, M. Brust and D. L. Cooper, *ACS Nano*, 2013, **7**, 8881–8890.

29 R. C. Murdock, L. Braydich-Stolle, A. M. Schrand, J. J. Schlager and S. M. Hussain, *Toxicol. Sci.*, 2008, **101**, 239–253.

30 J. J. Mittag, B. Kneidl, T. Preiß, M. Hossann, G. Winter, S. Wuttke, H. Engelke and J. O. Rädler, *Eur. J. Pharm. Biopharm.*, 2017, **119**, 215–223.

31 L. M. Herda, D. R. Hristov, M. C. Lo Giudice, E. Polo and K. A. Dawson, *J. Am. Chem. Soc.*, 2017, **139**, 111–114.

32 A. Bekdemir and F. Stellacci, *Nat. Commun.*, 2016, **7**, 13121.

33 C. Rocker, M. Potzl, F. Zhang, W. J. Parak and G. U. Nienhaus, *Nat. Nanotechnol.*, 2009, **4**, 577–580.

34 K. Voïtchovsky, N. Ashari-Astani, I. Tavernelli, N. Tétreault, U. Rothlisberger, F. Stellacci, M. Grätzel and H. A. Harms, *ACS Appl. Mater. Interfaces*, 2015, **7**, 10834–10842.

35 X. Chu, Z.-L. Zhao, G.-L. Shen and R.-Q. Yu, *Sens. Actuators, B*, 2006, **114**, 696–704.

36 N. Kim, D.-K. Kim and Y.-J. Cho, *Curr. Appl. Phys.*, 2010, **10**, 1227–1230.

37 G. Sener, E. Ozgur, E. Yılmaz, L. Uzun, R. Say and A. Denizli, *Biosens. Bioelectron.*, 2010, **26**, 815–821.

38 A. S. Pitek, D. O'Connell, E. Mahon, M. P. Monopoli, F. Baldelli Bombelli and K. A. Dawson, *PLoS One*, 2012, **7**, e40685.

39 M. P. Monopoli, D. Walczyk, A. Campbell, G. Elia, I. Lynch, F. Baldelli Bombelli and K. A. Dawson, *J. Am. Chem. Soc.*, 2011, **133**, 2525–2534.

40 S. Wei, L. S. Ahlstrom and C. L. Brooks, *Small*, 2017, **13**(18), DOI: 10.1002/smll.201603748.

41 H. Lopez and V. Lobaskin, *J. Chem. Phys.*, 2015, **143**, 12B620_621.

42 F. Gu, L. Zhang, B. A. Teply, N. Mann, A. Wang, A. F. Radovic-Moreno, R. Langer and O. C. Farokhzad, *Proc. Natl. Acad. Sci. U. S. A.*, 2008, **105**, 2586–2591.

43 S. Xu, B. Z. Olenyuk, C. T. Okamoto and S. F. Hamm-Alvarez, *Adv. Drug Delivery Rev.*, 2013, **65**, 121–138.

44 M. Colombo, L. Fiandra, G. Alessio, S. Mazzucchelli, M. Nebuloni, C. De Palma, K. Kantner, B. Pelaz, R. Rotem, F. Corsi, W. J. Parak and D. Prosperi, *Nat. Commun.*, 2016, **7**, 13818.

45 J. Kusunose, H. Zhang, M. K. J. Gagnon, T. Pan, S. I. Simon and K. W. Ferrara, *Ann. Biomed. Eng.*, 2013, **41**, 89–99.

46 N. Ucciferri, E.-M. Collnot, B. K. Gaiser, A. Tirella, V. Stone, C. Domenici, C.-M. Lehr and A. Ahluwalia, *Nanotoxicology*, 2014, **8**, 697–708.

47 A. S. Popel and P. C. Johnson, *Annu. Rev. Fluid Mech.*, 2005, **37**, 43–69.

48 S. Soleimani, M. M. Hasani-Sadrabadi, F. S. Majedi, E. Dashtimoghadam, M. Tondar and K. I. Jacob, *Colloids Surf., B*, 2016, **145**, 802–811.

49 F. Gentile, M. Ferrari and P. Decuzzi, *Ann. Biomed. Eng.*, 2008, **36**, 254–261.